Langmuir

ARTICLE

pubs.acs.org/Langmuir

Precision AFM Measurements of Dynamic Interactions between Deformable Drops in Aqueous Surfactant and Surfactant-Free Solutions

Hannah J. Lockie,[†] Rogerio Manica,[∥] Geoffrey W. Stevens,[†] Franz Grieser,[‡] Derek Y. C. Chan,[§] and Raymond R. Dagastine*[,†]

[†]Department of Chemical and Biomolecular Engineering, [‡]School of Chemistry, and [§]Department of Mathematics and Statistics, The University of Melbourne, Parkville VIC 3010, Australia

[∥]Institute of High Performance Computing, 1 Fusionopolis Way, 138632 Singapore

ABSTRACT: The atomic force microscope (AFM) has provided unprecedented opportunities to study velocity-dependent interactions between deformable drops and bubbles under a range of solution conditions. The challenge is to design an experimental system that enables accurate force spectroscopy of the interaction between deformable drops and thus the extraction of accurate quantitative information about the physically important force-separation relation. This step requires very precise control and knowledge of the interfacial properties of the interacting drops, the drive conditions of the force-sensing cantilever, the disposition of the interacting drops on the substrate and on the cantilever, and transducer calibrations of the instrument in order to quantify the effects of approach velocities and interfacial deformation. This article examines and quantifies in detail all experimental conditions that are necessary to facilitate accurate processing of dynamic force spectroscopy data from the AFM using the well-defined system of tetradecane drops in aqueous solutions under surfactant and surfactant-free conditions over a range of force magnitudes that has not been attained before. The ability of drops to deform and increase the effective area of interaction instead of decreasing the distance of closest approach when disjoining pressure exceeds the Laplace pressure means that the DLVO paradigm of colloidal stability as being determined by a balance of kinetic energy against the height of the primary maximum is no longer valid. The range of interfacially active species present in alkane-aqueous systems investigated provides insight into the applicability of the tangentially immobile boundary condition in colloidal interactions.

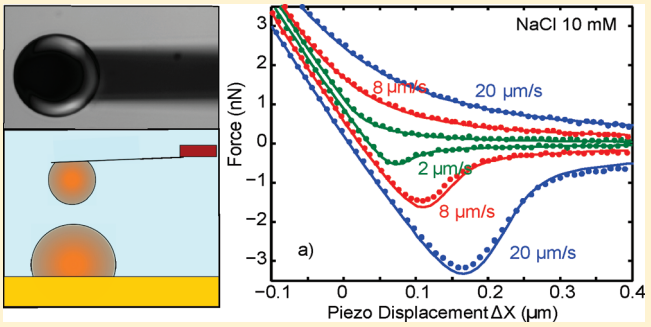

1. INTRODUCTION

Quantification of the dynamic or velocity-dependent interaction between two colliding emulsion drops in a continuous phase in terms of the force-separation relation is fundamental in the functional design and optimization of emulsion formulations. The spectrum of applications ranges from cosmetic product design[1−4] to enhancing taste sensation in food processing[5] to decontamination of pollution by heavy metal ions[6−8] and organics[9−12] to fine tuning emulsion-based metalworking fluids.[13,14] Such force-separation characteristics in dynamic interactions depend critically on the relative velocity of the interaction drops and concomitant variations in interfacial deformations that determine the effective surface area of interaction.

Over the past few years, the atomic force microscope (AFM) has been deployed to make direct measurement of the interaction force involving deformable drops and bubbles. The initial studies were equilibrium measurements using a solid colloidal particle probe on a bubble[15,16] or on an emulsion drop.[17−19] More recently, there have been a number of reports of measurements of nonequilibrium, velocity-dependent dynamic forces between alkane drops stabilized by surfactants[20−22] or proteins,[23] between a solid colloid particle probe and a tetradecane drop in the presence of surfactants,[24] between a bubble probe and a mica plate,[25] and between two bubbles in a concentrated aqueous electrolyte, focusing on the mechanism of bubble coalescence.[26] The intuition gained from such direct force measurements, particularly in relation to the coalescence of bubbles and drops, is consistent with coalescence studies of linear emulsion trains being transported in customized flow fields in microfluidic cells.[27,28]

It is important to note that force spectroscopy data from the AFM furnishes information on variations of the dynamic force with the relative displacement of the force-sensing cantilever. However during interaction, deformations of the interacting drops or bubbles can have a profound influence on the measured force, both in changing the effective areas of interaction as the

Received: December 9, 2010
Revised: January 12, 2011
Published: February 08, 2011

drops or bubbles approach or recede from each other and in changing the separation between the interfaces between which colloidal surface forces such as van der Waals, electrical double layer, and steric forces operate. In addition, at different velocities, the hydrodynamic pressure in the thin film of the continuous phase between the drops can also make a major contribution to interfacial deformations and determine the sign and magnitude of the measured force. A key element of such forces and deformations is the local separation between the interfaces of the interacting deformable colloids. The above complexities do not feature as centrally or indeed arise at all in dynamic force measurements between rigid, nondeforming bodies. For nondeforming bodies, the local shapes of the interacting surfaces do not vary and the absolute separation can be inferred from force spectroscopy data in the constant-compliance regime where the two interacting rigid bodies are in hard contact, corresponding to zero separation. With dynamic force measurements involving deformable bodies, hard contact is never realized so there is at present no direct experimental method of determining absolute separation. Furthermore, the local geometry of the interacting region between the interfaces can change very significantly during the course of the interaction, providing kinetic stability to the system.

In the velocity regime relevant to the AFM, hydrodynamic and surface forces tend to distort the deformable interfaces. However, capillary forces due to interfacial tension act to minimize the interfacial area and oppose deformations. Because the characteristic response time of capillary forces is short compared to the time scale of variations in hydrodynamic and colloidal surface forces, the Young-Laplace equation provides an accurate quantitative description of the deformational response of drops and bubbles with respect to the time-dependent perturbations in AFM experiments. On this basis, detailed theoretical modeling of both equilibrium[17,29−32] and dynamic[33−35] interactions in the AFM configuration becomes possible.

To use such models to extract precise quantitative information about the force-separation relation from AFM dynamic force spectroscopy data between deformable drops and bubbles, the values of a number of experimental parameters need to be controlled and determined accurately. These include the contact angle of the interacting drops on the substrate and on the cantilever, the behavior of the drops during the course of the interaction, particularly the drop on the cantilever, the effects of the drop positioning on the spring constant of the cantilever, and the mode of driving the cantilever using the AFM software. This article canvasses all of these issues in detail and reports on steps that need to be taken to facilitate the precise extraction of the important dynamic force-separation relation between deformable bodies from AFM dynamic force spectroscopy data using the available theory. This includes details of mixed self-assembled monolayers (SAM) used to provide a well-defined drop substrate. For force measurements, we use tetradecane drops in surfactant-free aqueous electrolyte solutions, a system that has not been studied previously, and in the presence of an anionic surfactant (sodium dodecylsufate, SDS) below and above the critical micelle concentration (cmc). We have also measured the magnitude of dynamic interaction forces over a range much larger than previously reported; up to 100 nN between drops of ~40 μm radius. Although it is possible to detect even higher apparent forces using the AFM, it is not possible to accept such data with confidence because the response of various components of the AFM would have exceeded their known calibrated region.

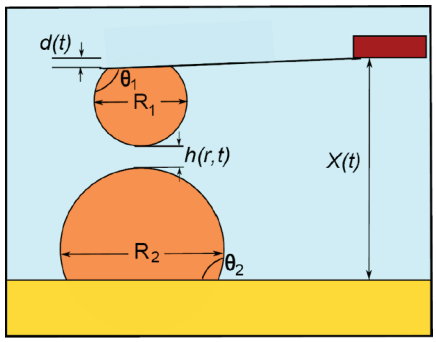

Figure 1. Schematic representation of the dynamic AFM force measurement system with drops immobilized on a gold-coated glass disk substrate and a custom-made AFM cantilever with a pattern-coated gold patch area.

In section 2, we detail the key experimental parameters that need to be quantified in AFM dynamic force measurements involving drops and the methods that we have developed to determine key system parameters accurately. A brief summary of the theoretical model used to analyze our results is given in section 3. In section 4, we present our measurements using tetradecane drops in aqueous electrolyte in the presence and absence of SDS and compare the results against predictions. This allows an investigation of the interfacial affinity of aqueous solution species under the no-slip boundary condition.

2. EXPERIMENTAL CONSIDERATIONS

In this section, we discuss the key experimental parameters that need to be determined to facilitate a quantitative interpretation of dynamic force spectroscopy data and report on the refinements of an experimental protocol that we have developed to eliminate uncertainties in such experiments.

A schematic representation of the AFM system used for all force measurements is shown in Figure 1. The interaction force is inferred from the deflection of the cantilever whose spring constant is measured independently. The cantilever deflection is measured by monitoring the position of a laser beam reflected from the back on the cantilever and is measured on a photodiode detector whose response is calibrated. The time-dependent interaction force between the drop on the cantilever and the drop on the substrate is measured as the end displacement of the cantilever, $X(t)$, is varied in a predetermined manner by a piezo electric motor. Deformations of the drop in the interaction zone and the local separation, $h(r, t)$, between the drops have to be determined from theory.

2.1. Cantilever Properties. The spring constant of the cantilever in air is obtained by the Hutter and Bechhoefer thermal spectrum method,[36] which is accepted to be the most reliable. For quantitative force-separation analysis of force spectroscopy data, it is clearly vital to determine the spring constant of the particular cantilever used in the experiment. Other calibration methods, such as the Sader method[37] that is based on simply measuring the resonance frequency and the quality factor of a cantilever and then inferring from these two measurements the cantilever spring constant using an empirical calibration formula, give unreliable results for some types of cantilevers. The reason is that the empirical calibration formula assumes that the spring constant of cantilevers with the same planar geometry and aspect ratio can be scaled by their planar dimensions. This assumption is based on the notion that the material properties along the thinnest dimension of the cantilever are uniform. Because of limitations in manufacturing tolerances, this assumption is not met in practice for cantilevers made from silicon nitride.[38,39] In a detailed study of over 100 V-shaped silicon nitride cantilever samples of the same shape fashioned from the same

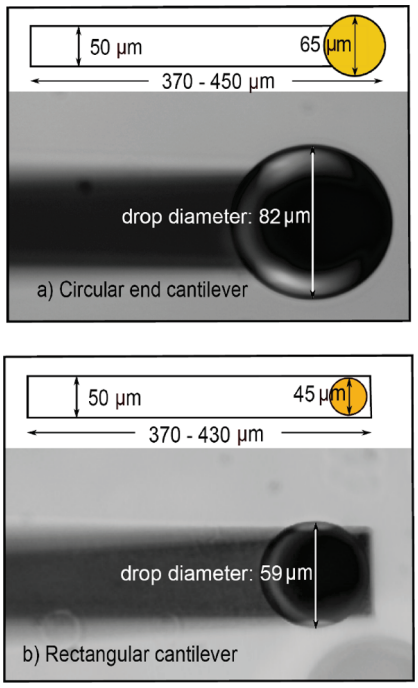

Figure 2. Optical microscopy image of a drop immobilized on a custom-designed tipless silicon cantilever with (a) a circular end cantilever with a hydrophobized gold patch and (b) a rectangular cantilever with a hydrophobized gold patch. The inserts show plan-view dimensions of the cantilever prior to drop attachment.

wafer,[40] the calibrated spring constant via the Sader empirical method can differ from the Hutter and Bechhoefer values by up to a factor of 2. Comparative studies on calibration methods also found variations of this magnitude for rectangular silicon nitride cantilevers.[41,42] Hence for precise force determinations, empirical calibration methods to determine the spring constant of a cantilever should be avoided.

It has been clearly established that when a particle probe,[43] and by deduction a drop, is attached to the cantilever for force measurement, the spring constant of this combination will vary by up to 20% from the Hutter and Bechhoefer value. The reason is that the position of attachment of the probe affects the point of load application on the cantilever and hence affects its effective spring constant. This situation can be alleviated by two refinements that we have adopted in this work. First, we used custom-manufactured rectangular tipless silicon cantilevers that were much longer (370−450 μm) than the drop diameters (50−65 μm) (Figure 2). Such cantilevers have more uniform and consistent material properties than the familiar silicon nitride cantilevers that have a triangular shape. The longer length also means that the spring constant will be less sensitive to the location of the particle or drop probe. Second, we pattern coated on the cantilevers gold circular anchoring patches at precisely known positions at the end of the cantilever for drop probe attachment. This alleviates possible uncertainties associated with the drop position in the cantilever. These gold patches were also hydrophobized to ensure that the oil drop probe was securely and accurately located on the cantilever throughout the experiment. In section 2.2, we discuss the details of the hydrophobic treatment process. We also used two different designs for the gold anchoring patches: (i) a circular patch of diameter 65 μm, which is slightly larger than the cantilever width (50 μm), that was attached to and extended beyond the end of the rectangular cantilever (Figure 2a) and (ii) a smaller circular patch located near the end of the cantilever that was wholly contained within the dimensions of the rectangular cantilever (Figure 2b). These refinements have allowed us to verify that the force-separation information derived from force spectroscopy data is independent of the type of cantilever used.

We note that in the dynamic AFM force measurement between rigid surfaces in the context of quantifying hydrodynamic slip at the solid surfaces, the cantilever geometry seems to have an anomalous role. Independent measurements using rectangular cantilevers[44] failed to detect appreciable hydrodynamic slip at solid surfaces, but measurements using triangular cantilevers[45] gave results that differed from those using rectangular cantilevers and the difference was attributed earlier to boundary slip.[46]

2.2. Drop, Cantilever, and Substrate Preparation. To measure the interactions between two drops of well-defined geometry, we require several drops positioned on a stationary substrate, one of which we are able to pick up and attach to the cantilever. Refinements were made to functionalize surfaces that facilitate drop pickup and to optimize the geometrical definition of the force measurement configuration. The surface chemistry of the cantilever gold patches and the substrate was carefully tailored to give different degrees of hydrophobicity.

A common method of hydrophobizing glass discs and cantilevers used in earlier AFM drop-drop experiments was to sputter coat surfaces with gold and then deposit self-assembled pure decanethiol monolayers on the surfaces.[20,21,24,47] This method provided hydrophobic surfaces with equivalent surface energies per unit area for the oil drops immobilized on the cantilever and the substrate. However, because the glass disk had a greater surface area than the cantilever gold patches, this system favored the oil drop remaining on the glass disk substrate. To facilitate drop transfer, the oil drop-cantilever surface interaction needs to be more favorable than the oil drop-substrate interaction. It has been shown that the variation in the composition of mixed thiol self-assembled monolayers on gold can be used to control the degree of hydrophobicity of surfaces with a high degree of consistency between similarly prepared surfaces.[48−50] In this work, we tailored the thiol chemistry at the gold-coated glass disk substrate (from which the drop is picked up) and at the cantilever gold patch surface to control the oil drop-substrate surface energy to facilitate efficient, highly repeatable experiments.

The silica glass discs with an rms roughness of 0.3−0.6 nm over 1 μm determined from AFM tapping-mode images were sputter coated with chromium (∼4 nm thick) and then with gold (∼6 nm thick). The rms roughness after coating was measured to be 0.3−1.6 nm over 1 μm. The surface was then immediately transferred to an ethanol solution of combined thiols for 18 h to allow the formation of a self-assembled monolayer (SAM) of mixed thiols at the surface (rms roughness after thiol coating 0.5−2.5 nm over 1 μm). Solutions were prepared to ensure precise control over the ratio of the hydroxyl-thiol (1-mercapto-1-decanol, Aldrich 99%) and alkane-thiol (decanethiol, Aldrich 98%) while allowing the total thiol concentration to vary between 1.8 and 2.1 mM, using stock solutions for different ratios. The key difference in surface preparation outlined here and in earlier methods[20,21,24,47] is that the addition of hydroxyl-thiol to the solution, and therefore the SAM, reduces the degree of hydrophobicity of the gold disk substrate compared to that of the SAM formed on the cantilever gold patch. The extent of hydrophobicity reduction of the glass disk SAM depends on the ratio of hydroxyl-thiol to alkane-thiols in the solution, and this can be quantified by contact angle studies.

Contact angle measurements were taken using a Data Physics (Germany) OCA 20 tensiometer system with tetradecane drops formed on the SAM-coated glass discs in aqueous solution. Mixed thiol monolayers have been classified extensively in terms of the contact angle of water and oil drops in air,[48−50] but little work has been done in studying the contact angle of oil drops at the surface in an aqueous phase. In excess of 25 discs, with 4 drops per disk, were used to verify that contact angles were consistent among discs prepared at similar thiol concentrations. An initial equilibration period of 5 min was allowed, and the contact angles were found to be constant within measurement error (±4°) over the following 30 min. This time frame is longer than the time

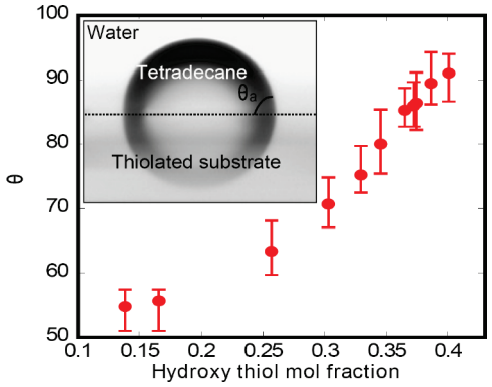

Figure 3. Average and maximum variation of contact angles (following equilibration) of tetradecane drops on thiol-coated substrates in Milli-Q water with varying ratios of alkane-thiol (decanethiol) and hydrolyl-thiol (1-mercapto-1-decanol) solution. (Inset) Optical microscopy image of a tetradecane drop on a thiolated substrate with equivalent hydrophobicity to that used in force measurements.

taken to carry out a series of force measurements for one solution condition. Variations of the equilibrium contact angle over a range of ratios of hydroxyl-thiol to alkane-thiol in solution are shown in Figure 3. The variation in the contact angle on discs prepared in like solutions was ±6°.

The concentration ratios in Figure 3 correspond to the thiol concentration ratio in the ethanol solution used to deposit the monolayer, which has been shown to differ from the surface concentrations of the self-assembled mixed thiol monolayer.[48−50] The solubility of the components is thought to have a large impact on the composition of the surface, with polar groups increasing the fraction that remains in solution. An analytical technique such as X-ray photoelectron spectroscopy (XPS) or ellipsometry can be used to determine the precise surface concentrations; however, this is not required in order to obtain a surface with a reproducible degree of hydrophobicity.

2.3. Drop Immobilization and Contact Control. In earlier work that deployed oil drop probes on triangular cantilevers,[20,24] there were limitations to specifying the precise positioning of the drops that can, as already mentioned, potentially impact the quantitative accuracy of the force-separation information that can be deduced. The cantilever modification with a gold patch, as discussed above, and the hydrophobicity modification detailed below have enabled long rectangular cantilevers to be used in drop-drop force measurements.

In the present refinement, the monolayer deposited at the cantilever gold patch is a pure alkane-thiol and therefore has maximum hydrophobicity for surfaces prepared using this method. When cleaned of any contaminants, the silicon regions of the cantilever reject the adhesion of the nonpolar oil, whereas the hydrophobized gold patch (insets in Figure 2) provides an energetically favorable and well-defined area for oil drop attachment.

As discussed earlier, the degree of hydrophobicity of the glass disk substrate must be lower than that of the alkane-thiol-coated cantilever gold patch to facilitate the transfer of drops stabilized at the surface to the cantilever. Drop immobilization was achieved through a controlled dewetting procedure to produce consistently micrometer-sized drops on a glass disk substrate in aqueous solution, as detailed in earlier work.[31] Briefly, the method involved spraying oil from a small-gauge needle syringe to create even drops on a hydrophobic surface. A clean O-ring is placed in the center of the disk, and aqueous solution is added slowly in ∼2-mm-diameter drops to form three large drops within the ring that are gradually allowed to coalesce. Through the controlled spreading of aqueous drops, oil drops are dewetted from the substrate with 15−80 μm drops remaining along the lines of intersection of the aqueous wetting fronts.

It was found that a minimum equilibrium contact angle on the gold-coated glass disk surface of approximately 80° was required to transfer a drop (30 to 40 μm diameter) to a cantilever. At higher alkane-thiol fractions (average contact angle of 85−92°), transfer improved substantially. At contact angles in excess of 92°, it was not possible to form stable drops at the surface for contact angle measurements. Consequently, there is an optimal contact angle window of 80−90° on the substrate that would facilitate both drop transfer to the cantilever and the formation of stable drops on the substrate to allow measurements of drop-drop interactions.

Force measurements under different solution conditions were made with the same drop pairs with solutions exchanged through the fluid cell of the AFM between measurements. Thus, consideration must be given to the effects of the additional solution species on the contact angle between the drops and the glass disk SAM. For instance, the addition of surfactant was found to reduce the degree of hydrophobicity of the thiol-coated disk, consequently increasing the contact angle. For example, the equilibrium contact angle of a tetradecane drop on a thiolated gold disk in pure water will increase from 80° to approximately 105° with increases in the solution concentration of SDS to up to 10 mM. At SDS concentrations of 0.1 and 1 mM, the drop contact angle change is less than 7°. Variations of the contact angles in the range of the aqueous systems used are given in Table 1.

2.4. Force Measurement. The AFM used in all experiments is an Asylum MFP-3D (Santa Barbara, CA) mounted on a Nikon TE-2000 inverted microscope with a completely enclosed fluid cell to prevent contamination during experiments, including solution exchange. The drops are aligned through optical microscopy and verified through force measurement by ensuring that the maximum force is obtained for a given piezo extension, indicating that the drops are interacting at their apexes. Individual force curves are taken in the single acquisition mode of the instrument, spaced by several seconds to ensure independent measurements, rather than driving the cantilever in continuous force-distance cycles above the drop. A large number (>40) of force curves are obtained for each drop-drop pair over a range of speeds to ensure the consistency of results and that the gradient of the force curve is unchanged, further validating a good alignment. However, individual curves displayed herein represent a single measurement without averaging or data smoothing.

In a typical force spectroscopy experiment, the cantilever position $X(t)$ is varied with a piezo motor driven by a set triangular voltage waveform. It is first decreased from an initial position during the approach phase and then increased during the retraction phase. Our AFM was equipped with a linear variable differential transformer (LVDT) that reported the position of the piezo drive as a function of time. The drive was operated in open-loop mode (to minimize potential noise) so that the LVDT $X(t)$ is the primary data that we used for the subsequent analysis of results. The high signal-to-noise ratio of the deformable interface system allows raw data to be used directly.

2.5. Zeta Potential. Measurements of electrophoretic mobility of the tetradecane drops were performed using a Malvern Zeta-Sizer 2000. Drop size measurement and analysis were performed via dynamic light scattering using a Malvern high-performance particle sizer (HPPS). Possible effects of multiple scattering were checked by comparing results at different emulsion concentrations at 0.1% (w/w) and 0.06% (w/w). Emulsions were prepared by vigorously shaking for 5 min in a Pyrex flask and then sonicating for 20 min to ensure monodispersity. The conversion of electrophoretic mobilities to zeta potentials was based on the Smoluchowski[51] formula for $\kappa a > 100$ (a = drop radius, $1/\kappa$ = Debye length) as in 10 mM NaCl systems. For lower values of κa, the methods of O'Brien and White[52] and Ohshima[53] were used. A summary of the results for tetradecane in aqueous-phase emulsion systems is given in Table 1.

2.6. Interfacial Tension. The interfacial tension was obtained from the pendant drop geometry measured using a Dataphysics OCA 20 tensiometer with a maximum error of ±2 mN/m.

Table 1. Measured Electrophoretic Mobilities, Drop Radii, and ζ Potentials of Tetradecane Drops at Different SDS and Salt Concentrations of the Aqueous Solution

solution	mobility ($cm^2\ V^{-1}\ s^{-1}$)	drop radius a (nm)[a]	Debye length κ^{-1} (nm)	average κa	ζ potential (mV)
0.1 mM SDS	-6.2 ± 0.7	122 ± 11	30	5	-80 ± 20
1 mM SDS	-7.0 ± 0.4	126 ± 18	9.6	13	-82 ± 10
10 mM SDS	-8.8 ± 0.4	111 ± 11	3.2	35	-124 ± 5
10 mM NaCl	-2.4 ± 0.2	370 ± 45	3.0	123	-31 ± 9

[a] Drop radius based on the number-average size distribution with low polydispersity as indicated by the distribution.

3. THEORETICAL MODEL

The theoretical model for the variation of the force, F, with the cantilever displacement, ΔX (Figure 1), between two interacting drops whose deformation is governed by the acting capillary forces is well established. Here we summarize results for equilibrium interactions, dynamic or time-dependent interactions, and also an analytical result valid in the regime when the drops have flattened against each other as a result of general repulsive interactions.

3.1. Equilibrium Force−Displacement Relation. The variation of the equilibrium force, F, with the cantilever displacement, ΔX (Figure 1), between two interacting drops whose deformation is governed by capillary forces can be generalized[54] from the particle-drop case.[30] Consider the general case of two dissimilar drops with constant interfacial tensions σ_1 and σ_2 and undeformed radii R_1 and R_2 for which the axisymmetric separation between the drop surfaces $h(r)$ obeys the augmented Young-Laplace equation,

$$\frac{1}{2}\frac{\overline{\sigma}}{r}\frac{\partial}{\partial r}\left(r\frac{\partial h}{\partial r}\right) = \frac{2\overline{\sigma}}{\overline{R}} - \Pi(h) \tag{3.1}$$

where

$$\frac{1}{\overline{R}} \equiv \frac{1}{2}\left(\frac{1}{R_1}+\frac{1}{R_2}\right) \quad \frac{1}{\overline{\sigma}} \equiv \frac{1}{2}\left(\frac{1}{\sigma_1}+\frac{1}{\sigma_2}\right) \tag{3.2}$$

Surface-force interactions are specified by the disjoining pressure, $\Pi(h)$. For the systems in this article, the disjoining pressure, Π, has contributions from electrical double layer interactions that we calculate from the nonlinear Poisson-Boltzmann theory and van der Waals interactions that can be estimated from Lifshitz theory. It turns out that for the salt concentrations and experimentally determined surface potentials given in Table 2 the drop-drop separation theory exceeds ~25 nm because of interfacial deformation. Hence the van der Waals contribution is negligible in this separation regime, and the electrical double layer contribution can be approximated by the superposition approximation.

In AFM experiments, the size of the interaction zone is small compared to the radii of the drops, thus the force between the drops is given by

$$F = 2\pi\int_0^\infty \Pi(h(r))r\ dr \tag{3.3}$$

By solving eq 3.1 with the condition $h(0) = h_o$ and the symmetry condition $dh/dr = 0$ from $r = 0$ and to some large value r_{max}, it can be shown that $h(r)$ has the asymptotic form[54]

$$h(r) \to h(0) + \frac{r^2}{\overline{R}} - \left(\frac{F}{\pi\overline{\sigma}}\right)\log\left(\frac{r}{2\overline{R}}\right) + 2H(\overline{R}),\ r \to r_{max} \tag{3.4}$$

where

$$H(\overline{R}) = \frac{1}{\overline{\sigma}}\int_0^\infty \Pi(h(r))r\log\left(\frac{r}{2\overline{R}}\right)\ dr \tag{3.5}$$

In practice, r_{max} will be outside the interaction zone between the two drops where the disjoining pressure, $\Pi(h)$, is negligibly small.

By analyzing the shape of the drop outside the deformation zone, one also obtains the result[54]

$$h(r) \to \Delta X + \frac{F}{K} + \frac{r^2}{\overline{R}} - \left(\frac{F}{2\pi\sigma_1}\right)\left\{\log\left(\frac{r}{2R_1}\right) + B(\theta_1)\right\} - \left(\frac{F}{2\pi\sigma_2}\right)\left\{\log\left(\frac{r}{2R_2}\right) + B(\theta_2)\right\} - \left(\frac{F}{2\pi\overline{\sigma}}\right),\ r \to r_{max} \tag{3.6a}$$

where

$$B(\theta) = \begin{cases} 1 + \frac{1}{2}\log\left(\frac{1+\cos\theta}{1-\cos\theta}\right) & \text{pinned } r_1 \\ 1 + \frac{1}{2}\log\left(\frac{1+\cos\theta}{1-\cos\theta}\right) - \frac{1}{2+\cos\theta} & \text{constant } \theta_0 \end{cases} \tag{3.6b}$$

The form of the function $B(\theta)$ depends on whether the three-phase contact line of the interacting drops is pinned at position r_1 or moves to maintain a constant contact angle θ_o. For the drop on the cantilever, the pinned r_1 condition is appropriate because the drop is constrained to sit on the hydrophobic gold patch on the cantilever. A comparison of experiment and theory indicates that a pinned r_1 condition also holds for the drop positioned on the thiolated glass disk substrate for all force measurements performed here. This is expected on the basis of the rms roughness measured over the surfaces (section 2.2).

The way to relate the force, F, to the AFM relative displacement is to integrate eq 3.1 from $r = 0$, for a given separation h_o, and calculate the force, F, and the quantity H using eqs 3.3 and 3.5 until their values have converged at some sufficiently large value of $r = r_{max}$. Then, eq 3.6 can be used to find the cantilever displacement, ΔX, corresponding to this force. The relative displacement, ΔX, is defined up to an arbitrary additive constant.

3.2. Nonequilibrium Force−Displacement Relationship. In a dynamic AFM experiment, the force, $F(t)$, now varies with time, t, as the cantilever displacement, $X(t)$, is varied with time. Therefore, in addition to the equilibrium disjoining pressure, Π, the hydrodynamic pressure, p, also contributes to the interaction in the Young-Laplace equation that describes the deformation of the position and time-dependent axisymmetric film of

dx.doi.org/10.1021/la1049088 |Langmuir 2011, 27, 2676–2685

thickness $h(r, t)$ between the drops

$$\frac{1}{2}\frac{\overline{\sigma}}{r}\frac{\partial}{\partial r}\left(r\frac{\partial h}{\partial r}\right) = \frac{2\overline{\sigma}}{\overline{R}} - \Pi(h) - p(r,t) \qquad (3.7)$$

The pressure, $p(r, t)$ and the film thickness, $h(r, t)$, are related by the Stokes-Reynolds equation that describes the film-thinning process. If the hydrodynamic boundary condition on the surfaces of the drops is tangentially immobile, then this equation has the form

$$\frac{\partial h}{\partial t} = \frac{1}{12\mu r}\frac{\partial}{\partial r}\left(rh^3\frac{\partial p}{\partial r}\right) \qquad (3.8)$$

where μ is the Newtonian shear viscosity of the aqueous continuous phase. We use the tangentially immobile hydrodynamic boundary condition because a vast majority of drainage experiments and dynamic force measurement results are consistent with this condition.[54] As we shall see, the results presented here are also consistent with the condition of tangentially immobile interfaces at the drop surfaces. The dynamic force between drops now includes the contribution from the hydrodynamic pressure

$$F(t) = 2\pi\int_0^\infty [\Pi(h(r,t)) + p(r,t)]r\,\mathrm{d}r \qquad (3.9)$$

Equations 3.7−3.9 now need to be solved with the initial undeformed profile: $h(r, 0) = h_o + r^2/\overline{R}$ and the symmetry conditions $\partial h/\partial r = 0 = \partial p/\partial r$ at $r = 0$ in the domain $0 \le r \le r_{max}$. The pressure decays as r^{-4} when $r \to \infty$, which is implemented as the condition $r(\partial p/\partial r)+4p = 0$ at $r = r_{max}$,[34] and the cantilever drive condition enters into the the final boundary condition[54]

$$\frac{\partial h(r_{max},t)}{\partial t} = \frac{\mathrm{d}X(t)}{\mathrm{d}t} + \frac{1}{K}\frac{\mathrm{d}F(t)}{\mathrm{d}t} - \frac{1}{2\pi\sigma_1}\frac{\mathrm{d}F(t)}{\mathrm{d}t}\left\{\log\left(\frac{r_{max}}{2R_1}\right) + B(\theta_1)\right\} - \frac{1}{2\pi\sigma_2}\frac{\mathrm{dF}(t)}{\mathrm{d}t}\left\{\log\left(\frac{r_{max}}{2R_2}\right) + B(\theta_2)\right\} \qquad (3.10)$$

Although force measurements will be reported at different nominal velocities, the actual displacement function, $X(t)$, as obtained by the LVDT attachment of the AFM is used in eq 3.10.[55]

3.3. High-Force Formula. If the interaction between the drops is repulsive, then the interaction zone between the drops will be flattened when the drops are pushed close together. In this limit, the force-cantilever displacement relation becomes independent of the approach velocity and is given by the formula[54]

$$\Delta X(t) \approx \frac{F(t)}{4\pi\sigma_1}\left\{\log\left(\frac{F(t)\overline{R}}{8\pi\overline{\sigma}R_1^2}\right) + 2B(\theta_1)\right\} + \frac{F(t)}{4\pi\sigma_2}\left\{\log\left(\frac{F(t)\overline{R}}{8\pi\overline{\sigma}R_2^2}\right) + 2B(\theta_2)\right\} - \frac{F(t)}{2\pi\overline{\sigma}} - \frac{F(t)}{K} \qquad (3.11)$$

where K is the spring constant of the cantilever.

This nonlinear relationship is important for two reasons. It demonstrates that the force-displacement relation is not linear, so the deforming drops do not behave as Hookean springs as assumed in earlier analyses of AFM data.[56,57] It is also a replacement of the constant compliance condition that holds for AFM force measurements between rigid surfaces.

It should be evident that in dynamic force measurements it may instructive to consider the force as a function of time because the force-displacement relation, $F(t)$ vs $\Delta X(t)$, actually depends on how the displacement, $\Delta X(t)$, is being driven. One may envisage that the piezo electric motor is used to drive the displacement, $\Delta X(t)$, at some nominal velocity. However, an examination of the LVDT data suggests that the nominal velocity is not constant and it is more precise to work with the experimental $\Delta X(t)$ function as reported by the LVDT attachment to the AFM in data analysis.

Table 2. System Parameters

solution	surface potential (mV)	interfacial tension (mN/m)	contact angle on substrate
0.1 mM SDS	−80 ± 20	44 ± 2	86 ± 6°
1 mM SDS	−82 ± 10	35 ± 2	88 ± 6°
10 mM SDS	−124 ± 5	10 ± 2	94 ± 6°
10 mM NaCl	−31 ± 9	53 ± 2	90 ± 6°

SDS System (0.1, 1, and 10 mM SDS)	
cantilever type	rectangular
drop radius on cantilever	35 ± 1 μm
drop radius on substrate	41 ± 1 μm
drop contact angle on cantilever	140 ± 2°
cantilever spring constant	0.287 ± 0.029 N/m (Hutter method)
AFM detector sensitivity	156 ± 10 nm/V

10 mM NaCl System	
cantilever type	circular end
drop radius on cantilever	39 ± 1 μm
drop radius on substrate	58 ± 1 μm
drop contact angle on cantilever	122 ± 2°
cantilever spring constant	0.086 ± 0.009 N/m (Hutter method)
AFM detector sensitivity	147 ± 10 nm/V
Hamaker constant: tetradecane-water-tetradecane[58]	8×10^{-21} J

4. RESULTS AND DISCUSSION

We have made dynamic force measurements using cantilevers with a circular end gold patch (Figure 2a,b) over a force range that is about 5 times larger than attained previously. The force-displacement results are found to be the same for similar experimental and system parameters, so we are confident that there are no artifacts associated with cantilever geometry. All system parameters of the experimental system are summarized in Table 2.

4.1. Dynamic Interactions in Surfactant. We have measured the dynamic force interactions between tetradecane drops at nominal velocities in the range of 1−40 μm/s. The aqueous phase contains the surfactant sodium dodecyl sulfate (SDS) in the concentration range of 0.1−10 mM, over which the aqueous−tetradecane interfacial tension varies in the range of 10−44 mN/m.

A comparison of force-displacement results for tetradecane drops in 10 mM SDS solution at low forces in the range of ±2 nN

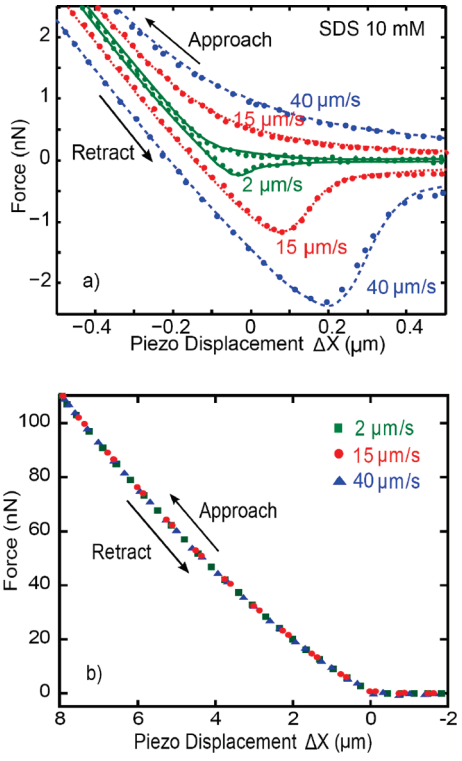

Figure 4. Measured force-cantilever displacement relation between tetradecane drops of radii 35 and 41 μm in 10 mM SDS. (a) Comparison of experimental force measurements (points) and theoretical predictions of the Stokes-Reynolds-Young-Laplace model of eqs 3.1−3.10 (lines) for different nominal velocities over the low force region where the effect of hydrodynamics is important. (b) High-force regime where the force-cantilever displacement relation becomes independent of the nominal velocity.

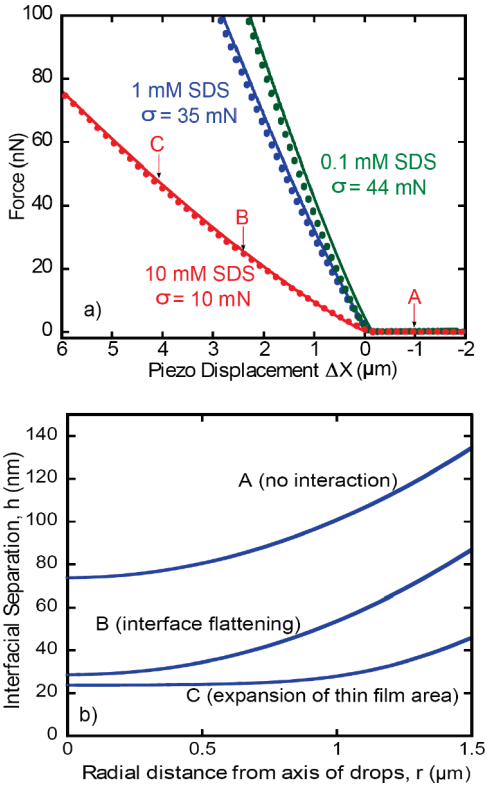

Figure 5. (a) Measured forces (points) between tetradecane drops of 35 and 41 μm radii in 0.1, 1, and 10 mM SDS compared to theory from eq 3.11 (lines) at a slow velocity of 2 μm/s. (b) Calculated interfacial separation as a function of the radial distance from the drop axis during the quasi-static interaction between drops in 10 mM SDS using the equilibrium model in eqs 3.1−3.6.

is shown in Figure 4a. Hereafter, for clarity, less than 5% of the experimental data points are plotted. At this SDS concentration, which is just above the critical micelle concentration, the disjoining pressure between the tetradecane surfaces is due to repulsive electrical double layer interactions that arise from the adsorbed anionic surfactant molecules. We see that the hysteretic effect between the approach and retraction branches of the force curves increases with increasing velocity, due to the increasing magnitude of hydrodynamic pressure. Predictions of the Stokes-Reynolds-Young-Laplace model of eqs 3.7−3.10 are shown to provide excellent agreement where all model parameters used are within the experimental uncertainties given in Table 2.

At higher forces of 5−100 nN, the force-displacement relations become independent of the nominal velocity (Figure 4b) and conform to the analytical relation given by eq 3.11. In the very high force region corresponding to a cantilever deflection of greater than 650 nm, the deflection against a solid surface becomes a nonlinear function of piezo travel; therefore, conversion of the AFM output to a force becomes inaccurate. To ensure the accuracy of the data, the deflection range is limited to below 600 nm of deflection. Depending on the spring constant of the cantilever, this corresponds to a maximum force limit of approximately 60−150 nN. This limit is considered in Figure 4, and all subsequent measurements are reported.

We exchanged the surfactant solution in the AFM fluid cell to study interactions at different SDS concentrations with the same pair of tetradecane drops retained on the cantilever and on the substrate. In Figure 5a, we show measured force-displacement results at 0.1, 1, and 10 mM SDS concentration at a nominal velocity of 2 μm/s for the same tetradecane drop pair. Over this large force range of 5−100 nN, the force-displacement data is independent of the nominal velocity (cf. results in Figure 4b), and the behavior is in accord with the predictions of the high-force formula in eq 3.11. The difference in the force at different SDS concentrations is accounted for by the SDS concentration dependence of the tetradecane-solution interfacial tension as indicated in eq 3.11. In Figure 5b, we show the separation between the interacting drops in 10 mM SDS aqueous solution, as deduced from eqs 3.1−3.6. This illustrates the degree of flattening in the interaction zone of the drops as the interaction force increases. The size of the interaction zone, ∼1 μm, is small compared to the drop radii (≥35 μm). Note that the separation between the drops does not fall below 20 nm; however, the extent of the flattened region increases with increasing force.

In Figure 6, we compare the results at lower SDS concentrations of 1 and 0.1 mM in the low-force region where hydrodynamic effects are important. Again, there is excellent quantitative agreement between experiment and theory with respect to the dependence of the dynamic force on the nominal velocity. Details of the evolution of the separation $h(r, t)$ between the tetradecane interfaces have been considered elsewhere.[24] At all SDS concentrations (10 mM down to 0.1 mM), theoretical fitting is performed with a no-slip boundary condition at the interface. This indicates that a small amount of adsorption of surface-active material at the interface is able to arrest the internal flow

dx.doi.org/10.1021/la1049088 |*Langmuir* 2011, 27, 2676–2685

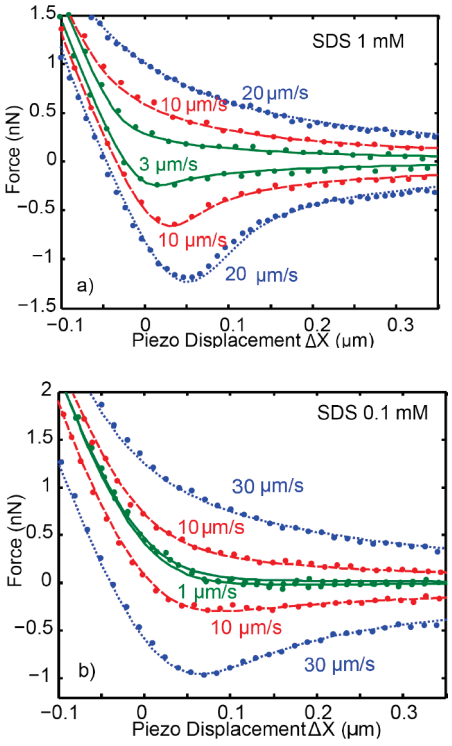

Figure 6. Measured forces (points) between tetradecane drops of 35 and 41 μm radii in (a) 1 and (b) 0.1 mM SDS compared to theoretical predictions of the Stokes-Reynolds-Young-Laplace model of eqs 3.1−3.10 (lines) at different nominal velocities.

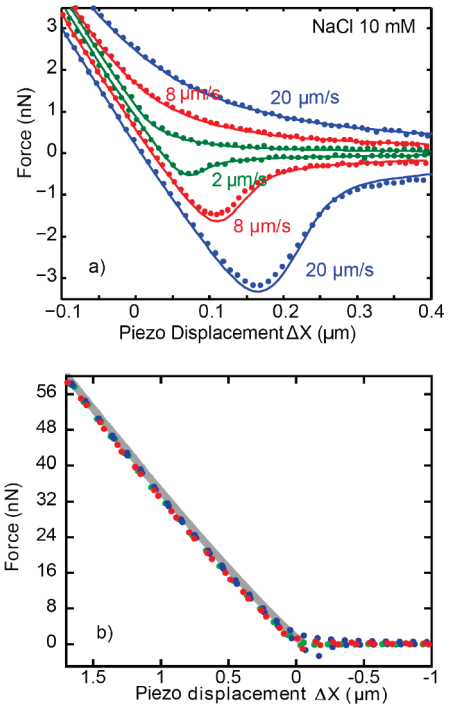

Figure 7. Forces between colliding tetradecane drops with radii of 58 and 39 μm in a 10 mM NaCl solution. (a) Comparison of experimental and theoretical forces at small forces. (b) The complete range of the force−displacement profile over forces at nominal speeds of 2, 8, and 20 μm/s (points) compares to the high-force formula (line) in eq 3.11.

completely through stress transfer; therefore, differences in the extent of interfacial adsorption have no effect on the interfacial mobility.

It should be noted that the potential mobility of a liquid-liquid interface (or internal flow) is a different mechanism for creating a nonzero tangential velocity at the surface than the mechanism commonly reported at hydrophobic solid surfaces,[59] where there is no flow on the solid side of the interface. Although the difference has been discussed in earlier work,[60] it can be a source of confusion in the literature.

4.2. Surfactant-Free Dynamic Interactions. It is well known that in the absence of added surfactant, oil drops in aqueous solution acquire a negative surface charge because of the preferential adsorption of hydroxyl ions at the interface. The resulting electrical double repulsion at low electrolyte concentrations is thought to be sufficient to stabilize drops against coalescence.[61] In Figure 7a, we see that the measured dynamic interactions between tetradecane drops in 10 mM NaCl, in the absence of added surfactants, are kinetically stable against coalescence for nominal speeds of 2−20 μm/s. The effects of hydrodynamic effects between the approach and retraction curves are evident over the low-force region, as for the surfactant-stabilized system. At higher forces, as in the presence of surfactants, the force-displacement relation is again independent of the nominal velocity and agrees with the high-force analytical formula given by eq 3.11 using independently measured parameters in Table 2. The spring constant value required is 20% higher than the average Hutter value measured (in accordance with earlier findings regarding the potential increase in spring constant values for loaded cantilevers[43]).

Close fitting of theory and experiment is provided for the nonsurfactant system using a nonslip boundary condition. The absence of slip in the 10 mM NaCl system cannot be explained through surfactant adsorption. This suggests that the interfacial adsorption of an ionic species, most probably the hydroxide ion,[61] is sufficient to arrest the transfer of stress across the interface during the drop-drop interaction.

It may be somewhat unexpected that the tetradecane drops remain stable in the absence of surfactants when the surface potential is relatively low: -31 ± 10 mV in 10 mM NaCl electrolyte. The colloidal stability of rigid parties, according to the Derjaguin-Landau-Verway-Overbeek theory, is determined by the height of the maximum of the interaction free energy between the particles given by the sum of the electrical double layer repulsion and the van der Waals attraction. That is, such a system is stable if the interaction energy maximum exceeds the thermal kinetic energy of the particles, $\sim(^3/_2)kT$. Under the Derjaguin approximation, which is applicable to particles in excess of 1 μm in size, the height of the maximum will be proportional to the particle size.

For deformable drops, the criterion for stability is different. As the drops can deform, they will do so as long as the disjoining pressure exceeds the Laplace pressure $(2\sigma/\overline{R})$ of the interacting drops (eq 3.1). Thus, when the drops are pushed together, instead of reducing the distance of closest approach between the drop surfaces as in the case of rigid particles, the drops will deform and flatten to increase their effective interaction area. Due to deformation, the separation h_{min} will remain the same (Figure 5) and will be given by the condition $\Pi(h_{min}) = 2\sigma/\overline{R}$. In other words, the drops can deform and increase the repulsive force between the drops by increasing the interaction area, enabling them to remain stable against coalescence as they are being pushed together. In Figure 8, we show that the surfaces

dx.doi.org/10.1021/la1049088 |*Langmuir* 2011, 27, 2676–2685

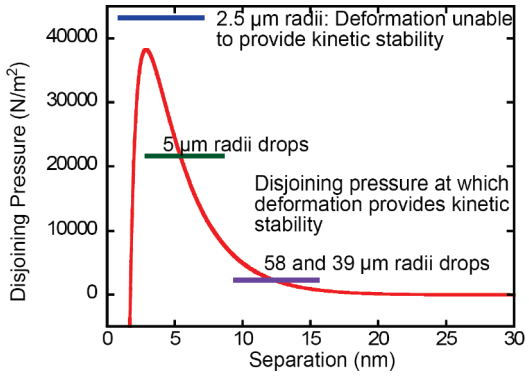

Figure 8. Variations of the disjoining pressure (Π) with the separation between two tetradecane interfaces in 10 mM 1:1 electrolyte.

of two drops of tetradecane of 39 and 58 μm radii in 10 mM 1:1 electrolyte cannot approach closer than about 12 nm, which is the separation at which the repulsive disjoining pressure is equal to the Laplace pressure. For two drops of 5 μm radius, the minimum separation is 5 nm, and very small drops (e.g., 2.5 μm radius) can have a Laplace pressure that exceeds the disjoining pressure maximum of about 40 kPa and hence cannot deform and will therefore be unstable.

5. SUMMARY AND CONCLUSIONS

A detailed consideration of system design and characterization, including contact angles, interfacial tensions, and precise drop positioning on a cantilever gold patch area and on a well-characterized substrate, has been undertaken. This has allowed well-defined measurements to be performed and matched very accurately with theory. The use of long silicon cantilevers allows confidence in the consistency of the detector sensitivity and the spring constant over a range of drop-drop interactions to higher forces than reported in earlier work. As forces were measured over a range of speeds and aqueous-phase conditions, we have been able to adjust independently measured parameters just once (within the bounds of individual parameter measurement errors) and theoretically model measured drop−drop interactions in a self-consistent manner.

Deformations are a vital consideration in the stability of soft matter systems and add complexity beyond the familiar DLVO theory used to describe rigid systems. Interfacial mobility, somewhat surprisingly, is not exhibited, with data both with surfactant and without surfactant showing a no-slip boundary condition during colloidal interactions. Indeed, a model that allows for interfacial mobility through internal flow would predict dynamic forces much smaller than that observed in the present experiment.[62] In the presence of surfactants, their adsorption at the interface provides a widely accepted physical explanation for rendering the interface immobile. In the absence of surfactant, we suggest that this may be due to ion adsorption at the interface, potentially the hydroxide ion (as suggested by others[61]), arresting the transfer of stress across the interface. The condition of immobility, even in the high-purity nonsurfactant system, suggests that water-emulsified micrometer-sized oil droplets do not experience greater rates of Brownian diffusion due to internal flow.

AUTHOR INFORMATION

Corresponding Author

*E-mail: rrd@unimelb.edu.au.

ACKNOWLEDGMENT

This work is supported by funding through the Australian Research Council and in part through the Particulate Fluids Processing Centre and the Australian Minerals Science Research Institute.

REFERENCES

(1) Tadros, T.; Izquierdo, R.; Esquena, J.; Solans, C. *Adv. Colloid Interface Sci.* **2004**, *108*, 303.
(2) Izquierdo, P.; Wiechers, J. W.; Escribano, E.; Garcia-Celma, M. J.; Tadros, T. F.; Esquena, J.; Dederen, J. C.; Solans, C. *Skin Pharmacol. Physiol.* **2007**, *20*, 263.
(3) de Morais, J. M.; dos Santos, O. D. H.; Delicato, T.; da Rocha, P. A. *J. Dispersion Sci. Technol.* **2006**, *27*, 1009.
(4) Sonneville-Aubrun, O.; Simonnet, J. T.; L'Alloret, F. *Adv. Colloid Interface Sci.* **2004**, *108*, 145.
(5) Malone, M. E.; Appelqvist, I. A. M.; Norton, I. T. *Food Hydrocolloids* **2003**, *17*, 775.
(6) Chakraborty, S.; Datta, S.; Bhattacharya, P.; Banerjea, S. *Sep. Sci. Technol.* **2006**, *41*, 771.
(7) Kalidhasan, S.; Rajesh, N. *J. Hazard. Mater.* **2009**, *170*, 1079.
(8) Sengupta, T.; Yates, M.; Papadopoulos, K. D. *Colloids Surf., A* **1999**, *148*, 259.
(9) Suchomel, E. J.; Ramsburg, C. A.; Pennell, K. D. *J. Contam. Hydrol.* **2007**, *94*, 195.
(10) Dar, A. A.; Rather, G. M.; Das, A. R. *J. Phys. Chem. B* **2007**, *111*, 3122.
(11) Cheng, H. F.; Sabatini, D. A. *Sep. Sci. Technol.* **2007**, *42*, 453.
(12) Childs, J. D.; Acosta, E. *J. Energy Res. Technol.* **2005**, *127*, 153.
(13) Cambiella, A.; Benito, J. M.; Pazos, C.; Coca, J.; Ratoi, M.; Spikes, H. A. *Tribol. Lett.* **2006**, *22*, 53.
(14) Kumar, D.; Daniel, J.; Biswas, S. K. *J. Colloid Interface Sci.* **2010**, *345*, 307.
(15) Ducker, W. A.; Xu, Z.; Israelachvili, J. N. *Langmuir* **1994**, *10*, 3279.
(16) Butt, H.-J. *J. Colloid Interface Sci.* **1994**, *166*, 109.
(17) Aston, D. E.; Berg, J. C. *J. Colloid Interface Sci.* **2001**, *235*, 162.
(18) Nespolo, S. A.; Chan, D. Y. C.; Grieser, F.; Hartley, P. G.; Stevens, G. W. *Langmuir* **2003**, *19*, 2124.
(19) Dagastine, R. R.; Chau, T. T.; Chan, D. Y. C.; Stevens, G. W.; Grieser, F. *Faraday Discuss* **2005**, *129*, 111.
(20) Dagastine, R. R.; Manica, R.; Carnie, S. L.; Chan, D. Y. C.; Stevens, G. W.; Grieser, F. *Science* **2006**, *313*, 210.
(21) Dagastine, R. R.; Stevens, G. W.; Chan, D. Y. C.; Grieser, F. *J. Colloid Interface Sci.* **2004**, *273*, 339.
(22) Gunning, A. P.; Mackie, A. R.; Wilde, P. J.; Morris, V. J. *Langmuir* **2004**, *20*, 116.
(23) Gromer, A.; Penfold, R.; Gunning, A. P.; Kirby, A. R.; Morris, V. J. *Soft Matter* **2010**, *6*, 3957.
(24) Webber, G. B.; Edwards, S. A.; Stevens, G. W.; Grieser, F.; Dagastine, R. R.; Chan, D. Y. C. *Soft Matter* **2008**, *4*, 1270.
(25) Manor, O.; Vakarelski, I. U.; Tang, X.; O'Shea, S. J.; Stevens, G. W.; Grieser, F.; Dagastine, R. R.; Chan, D. Y. C. *Phys. Rev. Lett.* **2008**, *101*, 024501.
(26) Vakarelski, I. U.; Manica, R.; Tang, X. S.; O'Shea, S. J.; Stevens, G. W.; Grieser, F.; Dagastine, R. R.; Chan, D. Y. C. *Proc. Natl. Acad. Sci. U.S.A.* **2010**, *107*, 11177.
(27) Bremond, N.; Thiam, A. R.; Bibette, J. *Phys. Rev. Lett.* **2008**, *100*, 4.
(28) Gunes, D. Z.; Clain, X.; Breton, O.; Mayor, G.; Burbidge, A. S. *J. Colloid Interface Sci.* **2010**, *343*, 79.
(29) Bhatt, D.; Newman, J.; Radke, C. J. *Langmuir* **2001**, *17*, 116.
(30) Chan, D. Y. C.; Dagastine, R. R.; White, L. R. *J. Colloid Interface Sci.* **2001**, *236*, 141.
(31) Dagastine, R. R.; Prieve, D. C.; White, L. R. *J. Colloid Interface Sci.* **2004**, *269*, 84.

(32) Dagastine, R. R.; White, L. R. *J. Colloid Interface Sci.* **2002**, *247*, 310.
(33) Manica, R.; Klaseboer, E.; Chan, D. Y. C. *Soft Matter* **2008**, *4*, 1613–1616.
(34) Carnie, S. L.; Chan, D. Y. C.; Lewis, C.; Manica, R.; Dagastine, R. R. *Langmuir* **2005**, *21*, 2912.
(35) Manica, R.; Connor, J. N.; Dagastine, R. R.; Carnie, S. L.; Horn, R. G.; Chan, D. Y. C. *Phys. Fluids* **2008**, *20*, 032101.
(36) Hutter, J. L.; Bechhoefer, J. *Rev. Sci. Instrum.* **1993**, *64*, 1868.
(37) Sader, J. E.; Larson, I.; Mulvaney, P.; White, L. R. *Rev. Sci. Instrum.* **1995**, *66*, 3789.
(38) Albrecht, T. R.; Akamine, S.; Carver, T. E.; Quate, C. F. *J. Vac. Sci. Technol.* **1990**, *8*, 3386.
(39) Martyniuk, M.; Antoszewski, J.; Musca, C. A.; Dell, J. M.; Faraone, L. *Smart Mater. Struct.* **2006**, *15*, S29.
(40) Webber, G. B.; Stevens, G. W.; Grieser, F.; Dagastine, R. R.; Chan, D. Y. C. *Nanotechnology* **2008**, *19*, 105709.
(41) Matei, G. A.; Thoreson, E. J.; Pratt, J. R.; Newell, D. B.; Burnham, N. A. *Rev. Sci. Instrum.* **2006**, *77*, 083703.
(42) Burnham, N. A.; Chen, X.; Hodges, C. S.; Matei, G. A.; Thoreson, E. J.; Roberts, C. J.; Davies, M. C.; Tendler, S. J. B. *Nanotechnology* **2003**, *14*, 1.
(43) Vakarelski, I. U.; Edwards, S. A.; Dagastine, R. R.; Chan, D. Y. C.; Stevens, G. W.; Grieser, F. *Rev. Sci. Instrum.* **2007**, *78*, 116102.
(44) Honig, C. D. F.; Ducker, W. A. *Phys. Rev. Lett.* **2007**, 98.
(45) Henry, C. L.; Craig, V. S. J. *Phys. Chem. Chem. Phys.* **2009**, *11*, 9514.
(46) Craig, V. S. J.; Neto, C.; Williams, D. R. M. *Phys. Rev. Lett.* **2001**, *87*, 054504.
(47) Clasohm, L. Y.; Vakarelski, I. U.; Dagastine, R. R.; Chan, D. Y. C.; Stevens, G. W.; Grieser, F. *Langmuir* **2007**, *23*, 9335.
(48) Bain, C. D.; Troughton, E. B.; Tao, Y. T.; Evall, J.; Whitesides, G. M.; Nuzzo, R. G. *J. Am. Chem. Soc.* **1989**, *111*, 321.
(49) Bain, C. D.; Whitesides, G. M. *J. Am. Chem. Soc.* **1988**, *110*, 3665.
(50) Bain, C. D.; Whitesides, G. M. *Science* **1988**, *240*, 62.
(51) Hunter, R. J. *Foundations of Colloid Science*; Oxford University Press: Oxford, U.K., 2001.
(52) O'Brien, R. W.; White, L. R. *J. Chem. Soc., Faraday Trans. 2* **1978**, *74*, 1607.
(53) Ohshima, H.; Healy, T. W.; White, L. R. *J. Colloid Interface Sci.* **1982**, *90*, 17.
(54) Chan, D. Y. C.; Manica, R.; Klaseboer, E. *Adv. Colloid Interface Sci.* **2011**; DOI:10.1039/C0SM00812E.
(55) Manor, O.; Vakarelski, I. U.; Stevens, G. W.; Grieser, F.; Dagastine, R. R.; Chan, D. Y. C. *Langmuir* **2008**, *24*, 11533.
(56) Ducker, W. A.; Xu, Z. G.; Israelachvili, J. N. *Langmuir* **1994**, *10*, 3279.
(57) Butt, H. J. *J. Colloid Interface Sci.* **1996**, *180*, 251.
(58) Prieve, D. C.; Russel, W. B. *J. Colloid Interface Sci.* **1988**, *125*, 1.
(59) Butt, H.-J.; Cappella, B.; Kappl, M. *Surf. Sci. Rep.* **2005**, *59*, 1.
(60) Dagastine, R. R.; Webber, G. B.; Manica, R.; Stevens, G. W.; Grieser, F.; Chan, D. Y. C. *Langmuir* **2010**, *26*, 11921.
(61) Beattie, J. K.; Djerdjev, A. M. *Angew. Chem., Int. Ed.* **2004**, *43*, 3568.
(62) Edwards, S. A.; Carnie, S. L.; Manor, O.; Chan, D. Y. C. *Langmuir* **2009**, *25*, 3352.